Seasonal Vegetation Response to Climate Variability on Land use Land Cover Changes using In-Situ and Satellite Imagery Observation Data for Semi-Arid Maasai Mara National Reserve Rangeland Ecosystem, Kenya

Charles C. Kapkwang [a,b*], Japheth O. Onyando [b], Peter M. Kundu [b] and Joost Hoedjes [c]

[a] *Department of Agricultural Bio Systems and Economics, University of Kabianga, P.O Box 2030-20200, Kericho, Kenya.*
[b] *Department of Agricultural Engineering, Egerton University, P.O Box 536-20115, Egerton, Kenya.*
[c] *Department of Water Resource and Earth Observation Science, University of Twente, Netherlands.*

Authors' contributions

Article Information

Original Research Article

ABSTRACT

Monitoring vegetation response through enhanced change detection by remote sensing and geographical information systems has tremendously improved real time information on surface features. Over the last few decades biomass monitoring at large scale has been made possible from information and metrics derived from satellite sensors. Maasai Mara National Reserve has been utilized in many decades as Kenyan natural grassland for wildlife grazing without periodic

Corresponding author: Email: ckewel2010@gmail.com, ckapkwang@kabianga.ac.ke;

assessment of biomass production as affected by impact of climate variability yet it's a tourism hub and one Kenyan economic contributor. This research evaluates the use of high spatial resolution satellite imagery such as the Moderate Resolution Imaging Spectro-radiometer or the Project for On-Board Autonomy–Vegetation and latest SENTINEL-2 for deriving the Normalized Difference Vegetation Index values in relations to in-situ measurements of biomass production between 2009 and 2019 in Mara, Kenya. Area frame sampling of biomass per unit area in $Kgha^{-1}$clipped from 50cm by 50cm quadrats were used in destructive sampling. The reserve grassland area coverage was estimated to be 717.203km^2 (46.75%) where the in-situ total above ground grass biomass projected in dry season was 35.094 tonha^{-1}. This was approximated as 2,516,952.208 tonnes per the season reserve cover while in wet season, 42.123 tonha^{-1} was approximated as 3,021,074.197 tonnes. The error matrices developed to assess the accuracies of the ecosystem classification indicated values that ranged between 80-100% and 87.5-100% for producer's and user's accuracy respectively. 3 out of 7 satellite imagery maps (2017, 2018, and 2019) were assessed for accuracy using reference data collected during fieldwork in 2018 and 2019 in ecosystem. The overall accuracy was 95.22% with Kappa index of 0.94 for 14 land cover classes shown in table 7. From the findings, potential factors influencing vegetation growth in different climatic regions are varied and complex. It can be noted that climate variability influence vegetation response in spatial scale to supply sustainable quality vegetation/pasture for wildlife feeds and ecosystem development. Vegetation mapping and monitoring of ecosystem behavior help stakeholders with information of vegetation characteristics Decision policy formulation and wildlife planning.

1. INTRODUCTION

Vegetation mapping and monitoring in semi-arid rangelands is extremely important as it gives the characteristics of variable supply of pasture/fodder for wildlife/livestock [1] which is largely attributed to low and erratic precipitation. In Kenya, some ecosystems have undergone irreversible changes because of grazing; some systems have degraded to the point where they can no longer support grazers [2]. Greater percent of Maasai Mara National Reserve (MMNR) grassland cover pose a threat of climate variability mainly during bi-seasonal periods (wet and dry) in that during normal wet seasons, most of these lands support large volumes of forage, which is also of relatively high quality [3]. The dry seasons, on the other hand, are characterized by scanty amounts of forage, which is mostly of poor quality [4]. This study however has used high temporal and spatial resolution satellite sensors and GIS data to compare the conventionally collected in-situ above ground grass biomass. The application of remote sensing (RS) and geographical information systems (GIS) data are currently the most common techniques used for analyzing surface features characteristic that aid in classification, enabling spatial planning, decision making and policy formulation works. The synthesis of MODIS imagery into high-quality, standard products available every 7, 8, or 16 days has greatly facilitated the use of satellite imagery for monitoring changes in rangeland landscapes among and within years [5]. The authors [6] predicted aboveground green biomass from MODIS net photosynthesis estimates throughout the growing season and characterized inter-annual variability in grassland vegetation. Climate variability leads to increased climatic uncertainty with variation in the weather pattern, mainly between seasons and years. In Europe permanent grasslands cover 33% and temporary grasslands cover 6%, respectively, of the total agricultural areas in Europe and land use land cover (LULC) vary between countries. Among terrestrial rangeland ecosystems, some are able to sustain populations of grazing animals while maintaining a stable-state of vegetation [7, 8, and 9]. In Kenya, the MMNR is globally unique and famous for the great wildebeest migration the largest and most species-diverse large mammal migration in the world, including 1.3 million wildebeest, 200,000 zebra and hundreds of thousands of Thomson's gazelle. According to [10], MMNR is one of the richest assemblages of wildlife in the world and supports about 237 herbivores per km^2, making it one of the most productive natural terrestrial ecosystems. This paper presents the statement of the problem, short literature review, materials and methods, results, discussion and finally, conclusion and future works of the study.

2. MATERIALS AND METHODS

2.1 Description of Studied Area

The Maasai Mara rangeland and ecosystem (Fig. 1) lies in southwest of Kenya and is approximately 1,510 square kilometers, of which less than 10% represents MMNR, while the rest is the unprotected land inhabited by the agro-pastoral community and conservancies. The area lies at an altitude of about 1,600 m above sea level, the Maasai Mara ecosystem is an area of undulating savanna/woodland intersected by numerous drainage lines and bisected by the Mara River [11]. The temperature range is 12 to 28^{0}C and annual rainfall normally lies within the range of 800-1,200 mm, with a northwest to southeast declining gradient. Rainfall is bimodal, with a main dry period from mid-June to mid-October and a shorter dry season during January and February.

2.2 Detecting and Quantifying Land Use and Land Cover Change

Land use is a description of how people utilize the land [12]. Land use establishes a direct link between land cover and the actions of people in their environment. Usually a rectangular quadrate frame is used to define the sampling area, although a quadrate can also be a permanently established area within a site. The most common quantitative sampling methods are the segment or quadrate method and the transect method. The quadrate method was adopted to allow the user to define a fixed area within which land use and cover could be measured. Area frame sampling usually attempts to define cover characteristics for an area much larger than the actual area sampled. For this reason, care must be taken to obtain samples that represent the entire habitat and that eliminate bias. Area frame sampling consists in "dividing the total area to be surveyed into N small blocks (Segments) without any overlap or omission, furthermore select a random sample of n small blocks and get the desired data for reporting units of the population that is in the sample blocks" [13]. Usually this means employing an experimental design that ensures random placement of the frame or permanent quadrat. Although small quadrates are much quicker to survey, they are likely to yield somewhat less reliable data than large ones. However, the larger quadrats require more time and effort to examine properly. A balance is therefore necessary between what is ideal and what is practical.

Fig. 1. Spatial distribution of biomass sampling campaign points in Maasai Mara National Reserve

2.2.1 Field clipping campaign of aboveground grass biomass

Aboveground grass biomass (AGGB) were harvested destructively at every end of the growing season (wet and dry) using hand-held shear to ground level via metallic square frame of dimensions 50cm x 50cm quadrat. Randomized complete block design was applied to collect AGGB from ten (10) spatially distributed sampling stations with six (6) replications for each site across the MMNR rangeland ecosystem. The "in situ" AGGB values were measured to provide data for calibration and validation of the satellite data. The coordinate reference points for individual quadrats of aboveground grass biomass clipped area were taken and recorded via Garmin geographical positioning system (GGPS). The clipped wet grass biomass from each quadrat was weighed using a digital balance, recorded, and stored in carrier bags. The samples were then taken to the laboratory where the moisture content was removed through oven drying. The dry matter of grass biomass was determined, hereafter referred to as derived aboveground grass biomass. Spatio-temporal and in-situ total aboveground biomasses for dry and wet season were annually computed for the entire rangeland ecosystem within the three consecutive years (2017 to 2019). The observed aboveground grass biomasses were averaged and values converted to tons per hectare.

The inside station treatments within the fenced Automatic weather station were used as the reference/control and those outside the station were used as the actual trial plots though accessible by wildlife feeding and interference. The clipped grass material (litter and standing parts) were manually separated immediately after harvest; wet weighed using a two (2) decimal digital balance, recorded and left spread to dry for a period of 7 days on sunlight and was alternatively oven dried for 72 hours at 60°C to constant weight. This was done to avoid further metabolism of the plant materials and to help determine its dry matter. The total aboveground grass biomass was considered the sum of dry litter and standing parts. The biomass performance of the dominant grassland per quadrat were observed twice for 2.5 years (30 months) period commencing from (May to December 2017) and from January to December (2018 - 2019). The standing AGGB were clipped and freshly weighed every onset and end of every wet and dry growth cycle each year using a methodology described by [14].

2.2.2 Direct expansion for area estimation

In MMNR rangeland ecosystems, Land Use Land Cover estimates were performed for several land covers, these were classified as grassland, sparsely distributed shrub-lands, cropland rain-fed, cropland irrigated and forest covers of various types such as closed and open evergreen and deciduous broadleaved cover. In the estimation of area with different land cover and use, stratified random sample formula developed by [15] was computed using equation (2.1) as follows:

$$\hat{T} = \sum_{i=1}^{h} \hat{T}(i) \qquad (2.1)$$

where,

$$\hat{T}(i) = D(i)\,\bar{y}(i), \quad \bar{y}(i) = \left[\frac{1}{n(i)}\right]\sum_{j=1}^{n(i)} y(i,j),$$

$$\hat{V}(\hat{T}) = \sum_{i=1}^{h}\hat{V}(\hat{T}(i)) = \sum_{i=1}^{h} D^2(i)\hat{V}(\bar{y}(i))$$

and $\quad \hat{V}(\bar{y}(i)) = \left[1 - \frac{n(i)}{N(i)}\right]\left[\frac{1}{n(i)}\right]\left[\frac{1}{(n(i)-1)}\right] \times \sum_{j=1}^{n(i)}\left[y(i,j) - \bar{y}(i)\right]^2$

here, h, is number of land use strata, $\hat{T}$, estimated total of land cover study zone, $\hat{T}(i)$ estimated total of study zone area for i^{th} stratum, $N(i)$, number of elementary area frame units in the ith stratum, $n(i)$, number of segments sampled in the ith stratum, $D(i)$,surface of the ith stratum, $\bar{y}(i)$. The average proportion of land cover area per segment in i^{th} stratum, $y(i,j)$, proportion of cover area in the jth sample in the ith stratum as deduced from digitization, $\hat{V}(\hat{T})$, estimated variance of $\bar{y}(i)$, $\hat{V}(\hat{T}(i))$, estimated variance of the total for the ith stratum and $\hat{V}(\bar{y}(i))$, estimated variance of $\bar{y}(i)$. It was paramount to note that in the direct expansion method, only the information deduced from the digitization of the segments are used.

2.2.3 Regression area estimation

The regression estimator consists of the corrections to estimated average variable Y as a function of the results obtained from an auxiliary variable X . In this study, for a given vegetation cover and each segment in the sample, Y is the proportion occupied by the crop/vegetation as deduced from digitization of the ground survey and X was the proportion of pixels of the satellite image classified as being of the given crop/vegetation cover. A linear regression was fitted in each stratum between the two variables. The linear model and the entire satellite image classification were used for regression estimation. The formulas found in [16] was used to estimate the total T using the following estimator,

$$\hat{T}_{reg} = \sum_{i=1}^{h} D(i)\, \bar{y}_{reg}(i), \text{ where, } \bar{y}_{reg}(i) = \bar{y}(i) + \hat{b}(i)\left[m_x(i) - \bar{x(i)} \right] \text{ and,} \qquad (2.2)$$

$D(i)$, surface of the ith stratum, $\bar{y}(i)$, the average proportion of land cover per segment in i^{th} stratum, $\hat{b}(i)$, the estimated regression coefficient for the ith stratum when regressing proportion of ground reported cover on proportion of classified pixels for the $n(i)$ sample units in the ith stratum,

$$\hat{b}(i) = \frac{\sum_{j=1}^{n(i)} \left[y(i,j) - \bar{y}(i) \right]\left[x(i,j) - \bar{x(i)} \right]}{\sum_{j=1}^{n(i)} \left[x(i,j) - \bar{x(i)} \right]^2} \qquad (2.3)$$

$m_x(i)$, the proportion of pixels classified as specific cover in the ith stratum,

$\bar{x}(i)$, the average proportion of pixels classified as specific cover per segment in the ith stratum, $x(i,j)$, proportion of pixels classified as specific cover in the jth sample unit in the ith stratum, The estimate variance for the regression estimator is given as;

$$\hat{V}(\hat{T}_{reg}) = \sum_{i=1}^{h} D(i)^2\, \hat{V}(\bar{y}_{reg}(i)$$

where,

$$\hat{V}((\bar{y}_{reg}(i)) = V(\hat{y}(i))\left[1 - \hat{r}(i)^2 \right] \qquad (2.4)$$

and $\hat{r}(i)^2$, sample coefficient of determination between the variables $y(i,j)$ and $x(i,j)$ in the ith stratum,

$$\hat{r}(i)^2 = \frac{\left\{\sum_{j=1}^{n(i)}\left[y(i,j)-\bar{y}(i)\right]\left[x(i,j)-\bar{x}(i)\right]\right\}^2}{\left\{\sum_{j=1}^{n(i)}\left[y(i,j)-\bar{y}(i)\right]^2\right\}\left\{\sum_{j=1}^{n(i)}\left[x(i,j)-\bar{x}(i)\right]^2\right\}}$$ (2.5)

Note that,

$$\hat{V}(T_{reg}) = \sum_{i=1}^{h} D(i)^2 \, \hat{V}(\bar{y}(i))\left[1-\hat{r}(i)^2\right] = \sum_{i=1}^{h} \hat{V}\left(\hat{T}(i)\right)\left[1-\hat{r}(i)^2\right] \text{ and so,}$$

$$\lim \hat{V}(\hat{T}_{reg}) \to 0 \text{, as } \hat{r}(i)^2 \to 0$$ (2.6)

If the coefficient of determination is large for most strata, it lowers the estimated variance for the regression estimator.

2.2.4 Relative efficiency

The success associated with the regression estimator was determined and its relative efficiency was calculated [16]. The RE of the regression estimator compared to the direct expansion estimator was defined as the ratio of the variances respective.

$$RE = \frac{\hat{V}(\hat{T})}{\hat{V}(\hat{T}_{reg})}$$ (2.7)

An $RE = 2$ means that the same precision would have been obtained if the ground data sample size had been doubled and the satellite image had not been used.

2.3 Satellite Imagery Data

2.3.1 Project for on-board autonomy – vegetation

The PROBA-V is a VEGETATION instrument has a Field Of View of 102^0, resulting in a swath width of 2295 km. This swath width ensures a daily near-global coverage (90%), whereas the full global coverage is achieved every 2 days. The central camera observes at 100 m nominal resolution, which covers a swath of about 517 km that ensures global coverage every 5 days. The author [17], indicated that PROBA-V observes in four spectral bands: BLUE (centered at 0.463 µm), RED (0.655 µm), NIR (0.837 µm), and SWIR (1.603 µm). Observations are taken at resolutions between 100 and 180 m at nadir and up to 350 m and 660 m at the swath extremes for the VNIR and SWIR channels, respectively. Final PROBA-V products are disseminated at 100 m, 300 m and, 1 km resolution.

The images for the years 2009 to 2019 were derived in GeoTiff format which were already corrected for radiometric and geometric distortions errors. The preprocessing steps in the workflow used Erdas imagine software 2014 and ArcGIS 10.1 software packages. These processes involved; layer stacking, Mosaicking, reprojection, sub-setting/clipping, classification, accuracy assessment done (using confusion matrix and ground truth data) and area change detection. Here, the radiometric processing converts the digital number count at a certain spectral band (DN) into physical TOA reflectance values. First, the DN number is corrected for detector non-linearities, dark currents, and inter-pixel non-uniformities. Secondly, these numbers are converted to sensor radiance L (Wm^{-2}sr^{-1}µm^{-1}), using the band-specific calibration coefficients derived from the radiometric ICP file. Finally, the TOA radiance L at a given spectral band is converted into TOA band reflectance using:

$$R_{TOA} = \frac{\pi \times d^2 \times L}{E_O \times Cos(\theta_s)}$$ (2.8)

With *RTOA* the obtained TOA reflectance value (-), *d* the Earth – Sun distance (AU), E_o the mean exo-atmospheric irradiance at the specific spectral band (Wm^{-2}µm^{-1}), with values from [18], and $\cos(\theta_s)$ the solar zenith angle (o). The

outputs of the radiometric processing are the Level 1C data.

2.3.1.1 Level 2 algorithm and data

The Level 1C data are used as input for further processing in the Level 2 processor, which consists of the following steps and the compositing procedure for the 300m and 1km products, differs in certain steps from level 2.

i).   Mapping and SWIR mosaicking
ii).   Snow/ice detection
iii).   Cloud and cloud shadow detection
iv).   Atmospheric correction

2.3.1.2 Cloud and cloud shadow detection

Clouds obstruct land surface parameter retrieval in satellite observations. Therefore, a proper cloud screening is pivotal in the pre-processing for the various value-added products. Many studies, as well as user feedback identified several issues with the Collection 0 PROBA-V cloud detection algorithm. The Collection 0 algorithm is based on the use of static thresholds applied to the BLUE and SWIR spectral bands. False cloud detection over bright surfaces, such as deserts and salt lakes, and flagging of thick ice clouds as 'snow/ice' were among the key problems of the operational cloud screening method. To overcome these limitations, a new algorithm was developed and implemented for the PROBA-V reprocessing (Collection 1).
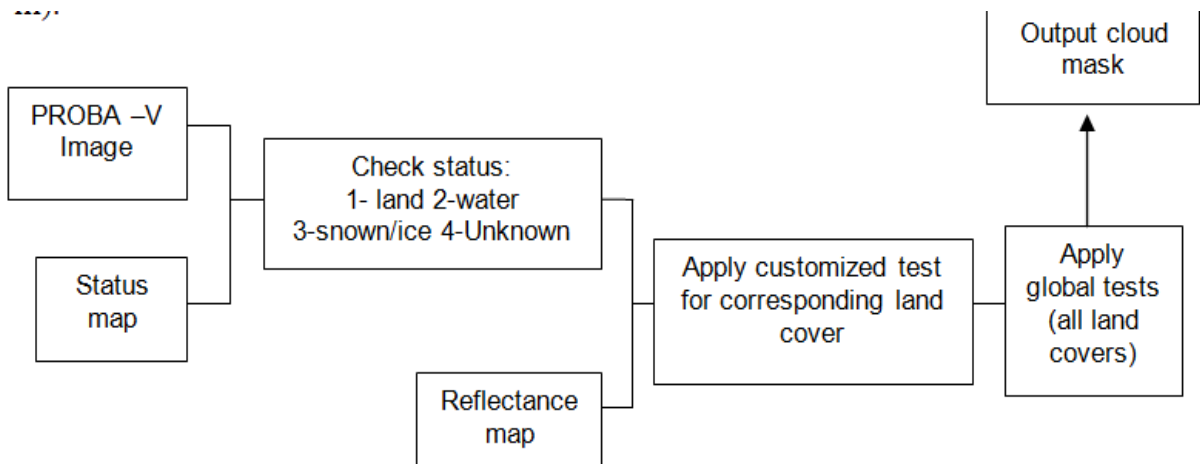
2.3.1.3 Collection 1 cloud detection algorithm

The improved and currently operational cloud detection algorithm addresses the main limitations of the Collection 0 cloud detection algorithm by using a more extensive and sophisticated set of cloud tests. A supervised training of a classification scheme that was designed to replace the operational Collection 0 algorithm.

i).   High-resolution surface albedo data are used as background reference maps.
ii). The decision to assign a pixel to 'cloud' or 'clear' is made via an extended set of threshold tests and similarity checks.

Table 1. PROBA-V spectral, radiometric, and geometric characteristics, Lref refers to the Top-Of-Atmosphere (TOA) irradiance at the respective spectral band, Geometric mean accuracy values obtained over the period 16 December 2016-15 December 2017. FWHM = Full Width at Half Maximum, SNR = Signal to Noise Ratio

Band name	Centre wavelength (µm)	Spectral range @ FWHM (µm)	SNR@ Lref (Wm^{-2} sr^{-1} µm^{-1}) at 300m resolution
BLUE	0.464	0.440 - 0.487	177@111
RED	0.655	0.614 - 0.696	598@110
NIR	0.837	0.772 – 0.902	574@106
SWIR	1.603	1.570 - 1.635	720@20

...).

Fig. 2. Flowchart of the collection 1 cloud detection algorithm

7
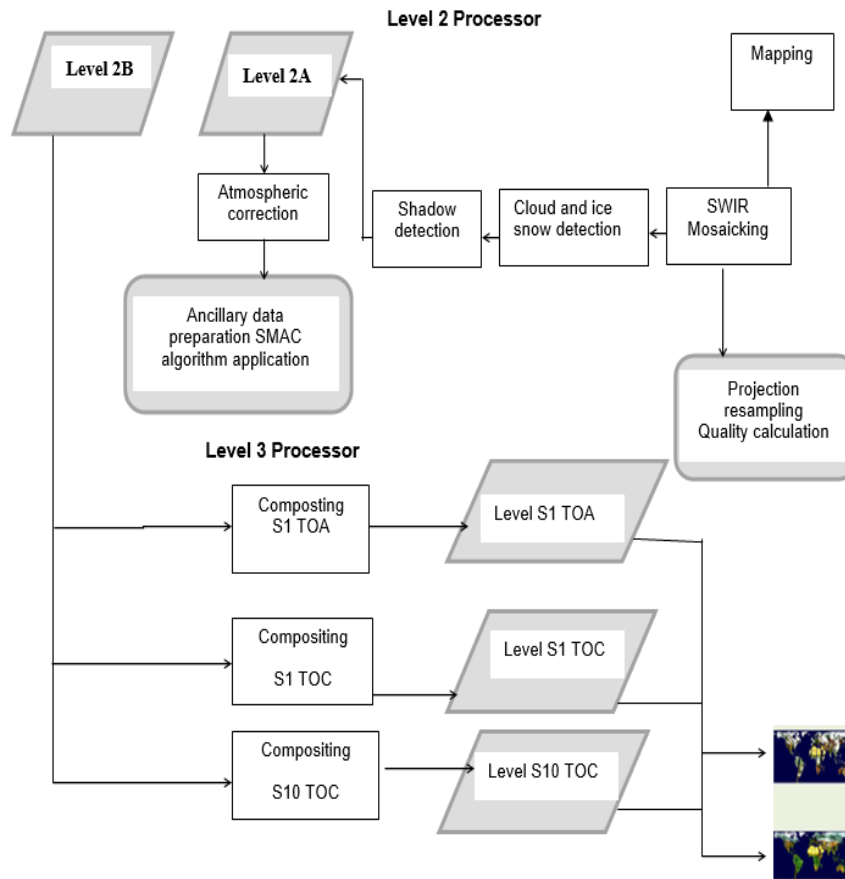
Fig. 3. PROBA-V product processing chain flowchart

2.3.1.4 Atmospheric correction

The Level 2A TOA reflectance observations are the resultant of surface reflectance and scattering, absorption, and multiple reflections within the atmospheric column below the satellite (clouds, gases, aerosols). In order to obtain the directional TOC reflectance values (Level 2B data), version 4.2 of the Simplified Model for Atmospheric Correction (SMAC), [19] is used. This model converts the observed TOA reflectance into TOC reflectance using auxiliary water vapour, ozone, and surface pressure data. Water vapour content is taken from the European Center for Mid-Range Weather Forecasts (ECMWF). Numerical Weather Prediction (NWP) model delivered by MeteoServices (http://www.meteoservices.be), which is bi-linearly interpolated in space and linearly in time. For ozone, a climatology based on 11 years of Total Ozone Mapping Spectrometer (TOMS) observations prepared by the Centre d'ÉtudesSpatialesde la Biosphère (CESBIO) is used. Surface pressure is derived from the Global Land Surface Digital Elevation Model

(GLSDEM), using a height to pressure conversion formula proposed by [20]. The aerosol optical thickness (AOT) is retrieved using an empirical relation between TOA NDVI and the SWIR / BLUE TOC reflectance ratio. This aerosol retrieval can only be applied for pixels with sufficient vegetation (NDVI > 0.2 and TOC SWIR < 0.4), for pixels, not fulfilling these criteria a simple AOT as function of the latitude is used [21].

2.3.2 Moderate resolution imaging spectro-radiometer

These MODIS instruments are designed to take measurements in spectral regions that have been used in previous satellite sensors. MODIS is adding to existing knowledge by extending datasets collected by heritage sensors such as the NOAA and AVHRR. The authors [22] used a combination of SPOT- Vegetation, Landsat long-term data record, and MODIS NDVI products to assess degradation and vegetation biomass changes in the Sahel region of Africa from 1982 to 2010. By extending these data sets, MODIS

promotes the continuity of data collection essential for understanding both long and short-term change in the global environment. MODIS provides data for land cover maps that tell scientists not only whether an area is vegetated, but also what kind of vegetation is growing there, separating coniferous forests from deciduous forests, or cropland from grassland. In addition to categories of vegetation, the maps recognize various non-vegetated surfaces, including bare soil, water, and urban areas land cover types in all MODIS's high quality. Daily measurements also allow scientists to track changes in land cover types and land use, to determine where forested land is becoming deforested, where grassland is becoming cropland, or where burned land is returning to natural vegetation. MODIS products were selected in a peer review process in 1992, based on scientific priorities established in the late 1980s. This was at a time when Mission to Planet Earth was a major science theme of NASA [23, 24]. The full resolution products from MODIS at 250, 500, and 1000 m are well suited to regional studies and when combined with Landsat data provide the basis for monitoring and modeling of land cover, land use change, and providing carbon observations [25] [26].

2.3.3 Sentinel 2A

Satellite images with a high temporal frequency (daily) but low spatial resolution (>250m) are frequently used for agricultural monitoring and applications when a high temporal resolution is needed. Sentinel-2A/MSI captures images of the earth's surface in 13 spectral bands at 10 m, 20 m and 60 m spatial resolution [27]. The improvement of peak NDVI estimation, GDD-based approach developed by [28], GDD application is used as proxy to predict an NDVI peak using historical relationship between NDVI and GDD. GDD is calculated as the average daily maximum ($T_{\max}$) and minimum temperatures ($T_{\min}$) minus a base temperature. Remotely sensed satellite data for crop area and yield estimation was used extensively in the United States and the EU, although significant applications have also been implemented in several developing countries [29] [30].

2.4 Normalized Difference Vegetation Index

The Normalized Difference Vegetation Index (NDVI) is a standardized index that allows the generation of an image displaying greenness (relative biomass). NDVI can also be particularly useful for predicting seasonal variability of ET and soil moisture status [31]. Seasonal and inter-annual global vegetation variability, reflected by normalized difference vegetation index (NDVI), assumes that NDVI contains clues about the vegetation response to climate change [32] [33]. This index takes advantage of the contrast of the characteristics of two bands from a multispectral raster dataset - the chlorophyll pigment absorptions in the red band and the high reflectivity of plant materials in the near-infrared (NIR) band. It is calculated from the measured intensities obtained in the red (R) and near infrared (NIR) spectral regimes. It is calculated as follows.

$$NDVI = \frac{\left(\rho_{nir} - \rho_{red} \right)}{\left(\rho_{nir} + \rho_{red} \right)} \qquad (2.9)$$

where, ρ_{nir} is near–infrared band reflectance, ρ_{red} is red band reflectance, red = Intensity/brightness of reflected light in the red filter (ca. 0.6–0.7 μm), nir = intensity/brightness of reflected light in the near infrared filter (ca. 0.8–0.9 μm).The NDVI - values are derived using MODIS and PROBA-V with their spectral reflectance in Band 3 (red band) reflectance and Band 4 (near-infrared reflectance). They are provided by the bands 4 and 8 of the Sentinel-2A MSI camera.

2.4.1 Accuracy assessment of classification

During the process of MODIS imagery classification, matrix errors mostly occur from the selection of training data. It was therefore needful to conduct an accuracy assessment on the derived land cover maps. This indicates the validity of the produced land cover maps because the classified maps and the ground truth are accounted for simultaneously. The author [34] has shown that accuracy assessment of a given region, future efforts of information were directed towards quantifying the dynamics of land cover. According to [35], the most common technique used is accuracy assessment of land cover classification for remotely sensed images in inter-rater reliability of error matrix (called confusion matrix, contingency tables, covariance matrix, or correlation matrix). The design of error matrix entails the comparison of classified data from land cover maps and the reference data (ground truth). The derived MODIS imagery

provided two options of comparison between the generated reference data using points generated randomly and the use of ground truth data that was taken from the field. The choice of MODIS image of 2000 was used to test the classification accuracy because the other options of EMT+ 2000 was far too old for comparison of the current reference data obtained. The table indicates the statistical techniques used to calculate the accuracy assessment of error matrix classes or components. The output of the classified images without any error or bias is the accurate thematic map. There are a number of equations that can show the level of error statistically such as producer accuracy, user accuracy, overall accuracy, and Kappa, which can be calculated using the error matrix [36]. An accuracy assessment was performed using collected ground-truth data for the two types of classification (rangeland and cropland) using a standard error matrix. Kappa statistics and overall accuracy were used to determine the performance of the selected methods of heterogeneous region (Table 2).

In reference to the description of [35], of error matrix components the accuracy assessments of the land cover classification were explained as follows;

i) Rows – These are the corresponding thematic classes in the ground truth map (training set)
ii) Columns – These are the thematic classes of the classified images.
iii) Diagonal Values – These represent the number of correctly classified pixels of each class (number of ground truth pixels with a certain class name that actually obtained similar to class name during classification.
iv) Off - diagonal values – corresponds to the misclassified pixels or the classification errors or the number of ground truth pixels that ended up in different class during classification. Following [37] approach, the applied statistical accuracy assessment in the study was described below;
v) Producer's accuracy - This corresponds to the fraction of correctly classified pixels with regard to all pixels of that ground truth class. Here, each class of the ground truth pixels (row), the calculated accuracy was done by dividing the number of correctly classified pixels by the total number of ground truth or test pixels of that class.

$$ACC = \frac{N_{1,1}}{N_{1+}} * 100\% \qquad (2.10)$$

where, ACC is the producer's accuracy, $N_{1,1}$ is the total number of the correctly classified pixels in that class and N_{1+} is the total number of ground truth pixels of that class (summation of the pixels in that row.

vi) User's accuracy (inter-rater reliability) - This corresponded to the fraction of correctly classified pixels with regard to all pixels classified as the classified image. In each classified image (column), to estimate its reliability calculations were done by dividing the number of correctly classified pixels by the total number of pixels that were classified in that class.

$$\mathrm{Re}l = \frac{N_{1,1}}{N_{+1}} * 100\% \qquad (2.11)$$

where Rel is user's accuracy(reliability), $N_{1,1}$ is the total number of the pixels classified in that category and N_{+1} is the total number of pixels that were classified as this category or class (summation of the pixels in that column).

vii) Overall accuracy – It is the summarized total agreement/disagreement between the classified and the training set data. It incorporates the major diagonal elements and excludes the commission and omission errors. The following expression was used.

$$OA = \frac{D}{N} * 100\% \qquad (2.12)$$

Where, OA is the overall accuracy, D is the total number of correctly classified pixels (diagonals values i.e. $N_{1,1} + N_{2,2} + N_{3,3} + \ldots + N_{n,n}$ and N_{OA} is the total number of the set (reference) pixels.

ix) Overall kappa statistic – This is the measure of agreement or accuracy based on KAPPA analysis. It is mainly used in comparing the classified data with the reference data (ground truth data) in determination of their significance difference. It can be expressed as follows;

$$\hat{K} = \frac{N_{OA} \sum_{i=1}^{n} N_{i,i} - \sum_{n=1}^{n} N_{i+} * N_{+i}}{N_{OA}^{2} - \sum_{i=1}^{n} (N_{i+} * N_{+i})} \qquad (2.13)$$

where $\hat{K}$ is the overall Kappa statistic coefficient, n is the number of rows in the error matrix, $N_{i,i}$

represents the total number of correct pixels in a class (value in row i and column i), N_{i+} is the total number of rows i, N_{+i} is columns total i and N_{OA} is the total number of the pixels in error matrix. The values greater than 0.7 indicates that the inter-rater reliability of classified and ground data were satisfactory. On the other hand, values less than 0.4 means fair agreement while 0.6 to 0.8 indicates substantial agreement.

3. RESULTS AND DISCUSSION

3.1 Measured Aboveground Standing Grass Biomass at Maasai Mara Rangeland Ecosystem

From Table 3, it can be seen that during the dry season in 2017, the observed aboveground grass biomass (AGGB) measured an average dry biomass weight of 0.328 kg/m^2 or 3.28 tons/ha obtained from Randomized Complete Block Design (RCBD) with six replicated (0.5m by 0.5m) quadrats each had slight biomass variations. The aboveground biomass from a similar site on a wet season in 2017 also varied slightly with an average weight on dry matter basis as 1.634 kg/m^2 or 10.208 tons clipped from 2.5m by 2.5m quadrat. The standard deviation was 0.0508 kg/m^2 while the standard error of the mean was ±0.0376.

From seasonal quantitative analysis of vegetation coverage in both seasons shown in Tables 3 and 4, there was 79.92 % high vegetation coverage class in the year 2018 wet season. In the year 2018, there was heavy rainfall, which fell almost throughout the year, and the above ground biomass harvested were dried and measured from each quadrat and the results were high as compared to 2017.Yearly wet seasons were characterized with high vegetation cover classes from highest to lowest 2018 (79.92%) and 2017 (20.07%) consecutively. During the dry season, low

vegetation coverage class was in 2017 experienced because of low and short rainy seasons. Land generally occupied by MMNR rangeland ecosystem covers 1,534km^2 and the area covered as grassland were estimated to be 717.203km^2 (46.75%) where the total AGGB during the dry season was 35.094 tonha^{-1} that translate to seasonal quantify of 2,516,952.208 tonnes while during the wet seasonal AGGB was 42.123 tonha^{-1} corresponding to 3,021,074.197 tonnes biomass. These conversions were based on MMNR land cover during the bi-seasonal period when vegetation density was at its low and maximum productivity; however the quantity may not be precise because of continuous wildlife feeding with adverse effect of migratory largest wilderbeest population during sampling. Similar observations were made by [38], where household density, distance to road, grass biomass, livestock and wildlife density had a normal distribution centered around the mean and standard deviation of each variable in Amboseli and Mara ecosystems. Further observation from these models, indicates a low wildlife density trend in neighboring private land tenure as compared to communal and government land that depict higher wildlife density in wet years relative to dry years.

Fig. 4 indicates that during the wet periods, green grass biomass was high as compared to dry season. There was better biomass coverage on the upper catchment area such as Mara main station, Olimisiogioi, Upstream and Helicopter and most of them were homogeneously distributed with green biomass cover across the rangeland with scarce scenery of mixed shrubs and tall trees along the river channels and streams passing across the rangeland. On lowlands toward Mara Bridge with low altitude (1520m), there was less vegetation/grass coverage in the western and southern periphery of the catchment while, better grass vegetation coverage were observed in the northern part of MMNR ecosystem.

Table 2. Design of Confusion/Error Matrix applied in accuracy assessment of land cover classification

| | Class | Reference data | | | | | |
		A	B	C	……	n	Row Total
Classified Data	A	$N_{1,1}$	$N_{1,2}$	$N_{1,3}$	……	$N_{1,n}$	N_{1+}
	B	$N_{2,1}$	$N_{2,2}$	$N_{2,3}$	……	$N_{2,n}$	N_{2+}
	C	$N_{3,1}$	$N_{3,2}$	$N_{3,3}$	……	$N_{3,n}$	N_{3+}
	…..	…….	……	……	……	……	…..
	n	$N_{n,1}$	$N_{n,2}$	$N_{n,3}$	……	$N_{n,n}$	N_{n+}
	Column Total	N_{+1}	N_{+2}	N_{+3}	……..	N_{+n}	N_{OA}

Table 3. Above ground standing biomass measured from spatially distributed Maasai Mara catchment sites during dry season (2017)

Location	Coordinates Latitudes Longitudes		Quadrat Area in m^2	Average Wet wgt (Kg)	Average Dry wgt (Kg)	Average Projected biomass in tons/hac	Average Biomass in Kg/m^2	Standard Deviation	Standard Error
Mara Main	-1.49332	35.14918	0.25	2.663	2.053	3.284	0.328	0.0508	± 0.038
Kissinger	-1.55889	35.23664	0.25	0.190	0.092	3.660	0.366	0.0290	± 0.012
Ashnil	-1.45291	35.07215	0.25	0.198	0.093	3.710	0.371	0.0273	± 0.011
Helicopter	-1.53042	35.17422	0.25	0.172	0.097	3.890	0.389	0.0211	± 0.008
Talek	-1.46117	35.18276	0.25	0.148	0.089	3.570	0.357	0.0346	± 0.014
NiceBridge	-1.49519	35.19034	0.25	0.185	0.092	3.600	0.360	0.0123	± 0.050
V-section	-1.46249	35.10616	0.25	0.182	0.089	3.550	0.355	0.0246	± 0.010
Upstream	-1.52919	35.23824	0.25	0.148	0.089	3.540	0.354	0.0316	± 0.013
Olimisiogioi	-1.50384	35.12008	0.25	0.148	0.090	3.650	0.365	0.0178	± 0.007
Mara Bridge	-1.53833	35.03615	0.25	0.143	0.066	2.640	0.264	0.0312	± 0.013
Total AGB			35.094	0.351					

Table 4. Above ground standing biomass measured from spatially distributed Maasai Mara catchment sites during wet season (2018)

| Location	Coordinates Latitudes	Longitudes	Quadrat Area in m^2	Average Wet wgt (Kg)	Average Dry wgt (Kg)	Average Projected biomass in tons/hac	Average Biomass in Kg/m^2	Standard Deviation	Standard Error
Mara Main	-1.49332	35.14918	0.25	1.784	0.255	6.540	0.654	0.1714	± 0.0700
Kissinger	-1.55889	35.23664	0.25	0.353	0.147	5.890	0.589	0.1304	± 0.0532
Ashnil	-1.45291	35.07215	0.25	0.400	0.109	4.370	0.437	0.2550	± 0.1041
Helicopter	-1.53042	35.17422	0.25	1.768	0.103	4.133	0.413	0.0149	± 0.0061
Talek	-1.46117	35.18276	0.25	1.732	0.103	4.120	0.412	0.0136	± 0.0056
Nice Bridge	-1.49519	35.19034	0.25	1.801	0.104	4.140	0.414	0.0100	± 0.0041
V-section	-1.46249	35.10616	0.25	1.865	0.103	4.110	0.411	0.0121	± 0.0049
Upstream	-1.52919	35.23824	0.25	1.932	0.106	4.230	0.423	0.0225	± 0.0092
Olimisiogioi	-1.50384	35.12008	0.25	1.565	0.099	3.970	0.397	0.0165	± 0.0067
Mara Bridge	-1.53833	35.03615	0.25	0.346	0.077	3.080	0.308	0.0460	± 0.0188
Total AGB					**42.123**	**0.421**			
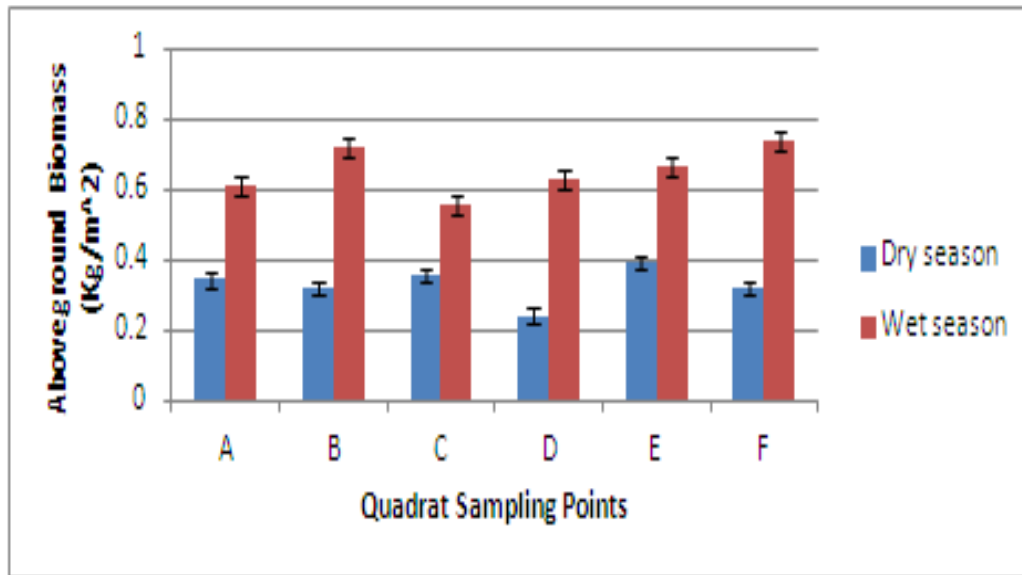
Fig. 4. Box plot of selected trend of Mara main aboveground biomass per quadrat during dry and wet season

3.2 Normalized Difference Vegetation Index (NDVI)

Spatial monthly values of NDVI were derived from MODIS, PROBA-V and SENTINEL-2 imagery for the entire rangeland within the period of study (2017- 2019). The images displayed in Figs. 5 and 7 are the sequential bi-seasonal images of (a) wet and (b) dry periods when site's aboveground biomass measurements were clipped and sampled for oven drying to determine dry matter content (biomass). Measured AGGB indicates similar corresponding range of NDVI values with transition in which vegetation greenness occurs for the period of 2017, 2018 and 2019 wet seasons. High NDVI value shows that there is high surface spectral reflectance due to greenness and high-density vegetation cover while low NDVI value indicates low or sparsely distributed vegetation cover with low density in greenness. The observed images shown that during the dry season, low vegetation greenness was realized and high vegetation greenness in wet season.

The Fig. 5 indicates greenness within the spatial segments in the month of May wet season with spectral reflectance ranged of between 0.263 and 0.841. During the dry season the greenness of vegetation particularly grass aboveground biomass spectral value ranged between 0.247 and 0.831 which shown that during the dry period the vegetation greenness was lower than during the wet season. This indicates that the bloomy vegetation cover was well dense during the wet season because of sufficient soil moisture useable by plants growth and development. As observed from Fig. 7, May and December NDVI greenness on the upper left catchment of the rangeland ecosystem, the greenest vegetation is relatively high on May as compared to the December period.

From Figs. 6 and 7, it can be observed that the spectral reflectance for greenness indicates high blossom vegetation occurrence between 0.663 μm and 0.828 μm during the wet season in 2019 while dry seasons ranged between 0.775 μm and 0.886 μm in December of the same year. The trend of NDVI derived from MODIS imagery satellite data displayed surface features and reflects information of wet (May) and dry season (Dec) acquired on consecutive years in (May and Dec, 2017, 2018 and 2019). Observation made shows that during dense greenness period, there was high rainfall, which corresponded to high soil moisture content availability. This shows that the available soil moisture was utilized for vegetation growth and development where the net resultant effect was high biomass density. The NDVI ranged between 0.117 to 0.0668 in May and Dec 2019 respectively. The authors [39] used related time series of MODIS NDVI to observe changes in overall plant biomass across years and to changes in plant functional group responses within years.
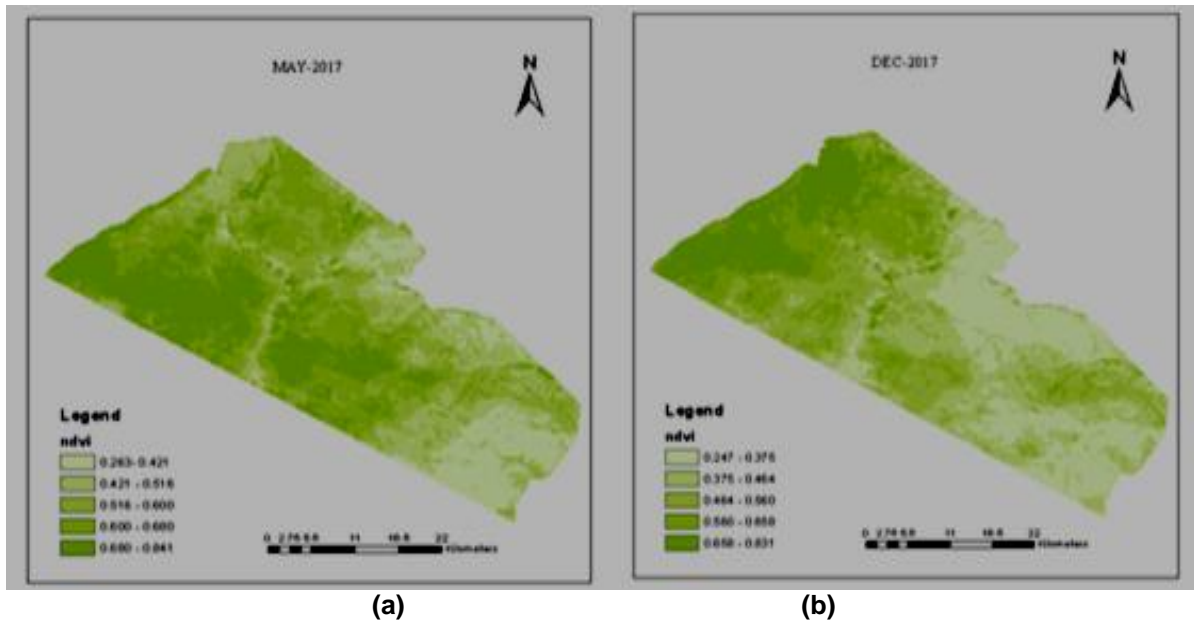
Fig. 5. Vegetation NDVI trend from MODIS satellite imagery data for Maasai Mara Rangeland wet and dry season acquired on (May and Dec 2017)
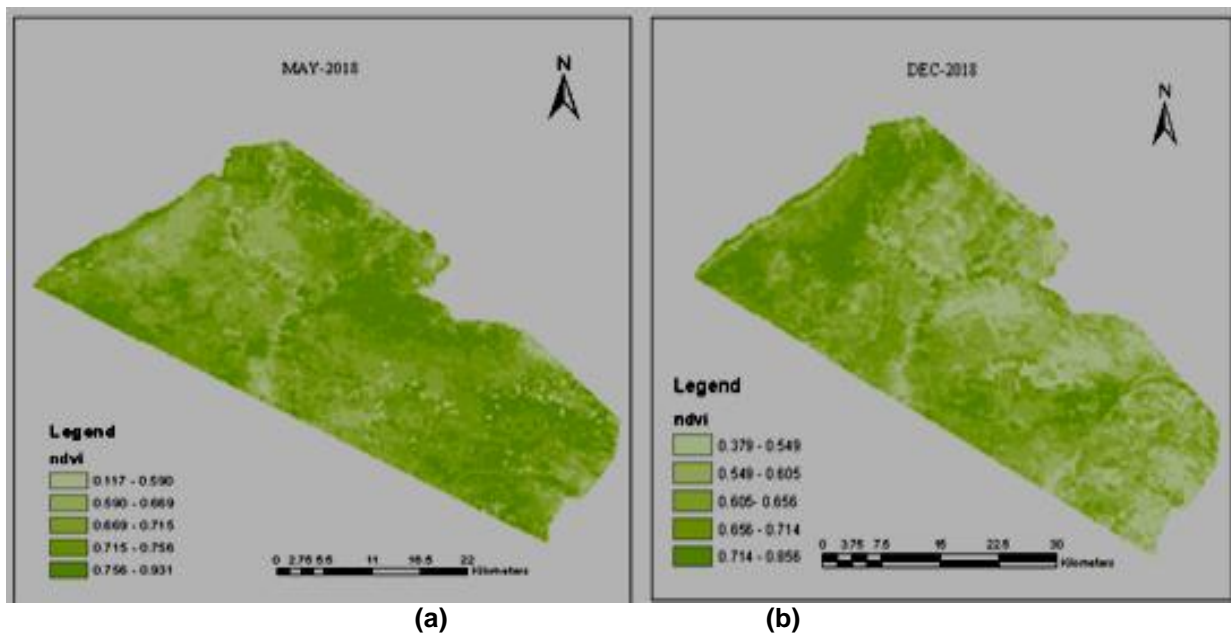

Fig. 6. Vegetation NDVI trend from MODIS satellite imagery data for Maasai Mara Rangeland wet and dry season acquired on (May and Dec 2018)

3.2.1 Time series analysis of minimum and maximum NDVI

Based on the study, the three years period of 2017, 2018, and 2019 indicated in Figs 5, 6 and 7, maximum and minimum vegetation cover indicates homogeneity trend though low minimum and maximum vegetation cover in the dry season between the months of December, January, and February cutting across the consecutive years. The maximum vegetation cover was observed in the month of March running through July, September, October, and November in 2018. The vegetation cover variation relied mainly on the seasonal rainfall that fell due to the effect of East Africa intertropical convergence zone (ITCZ). During the rainy season, most of the rainfall events in

15

2017, 2018, and 2019 indicated that the maximum NDVI values were below 0.5 within the initial two months before the onset of the wet season. This was followed by increased NDVI values caused by greenness of vegetation cover between the range of 0.753 and 0.999 while there was a reduction in maximum NDVI values in the dry period ranged between 0 and 0.200 caused by decrease in rainfall followed by subsequent decline in vegetation greenness across the entire rangeland ecosystem.

3.2.2 Linear correlation between mean monthly ndvi and mean maximum monthly rainfall

The relationship between seasonal precipitation and NDVI was very strong and predictable when observed at the appropriate spatial and temporal scale. The phenology of vegetation in all formations closely reflects the seasonal cycle of rainfall. Within the period 2017-2019, there was considerable monthly, seasonal, or year-to-year variation in precipitation and NDVI throughout the region of MMNR rangeland ecosystem. The yearly correlation coefficients between NDVI and precipitation are very high, while the correlation between NDVI and temperature are low. The total growing season analyses show that the general temporal or spatial distribution of NDVI in the whole study area corresponds directly with the spatial pattern of average monthly or annual precipitation. Annual rainfall in 2018 was relatively high as compared to 2017 and 2019, this was depicted by aboveground biomass harvested in wet season in 2018 as compared to biomass harvested during wet, and dry season in 2017. During the dry season NDVI coefficient of variation analyses showed high instability or variability in 2017 erratic precipitation episodes.

3.2.3 Time series analyses of mean monthly rainfall for 2017-2019 period in maasai mara rangeland ecosystem

Rainfall variability in this region through time was erratic almost throughout the whole period of study in seasons of wet and dry spells (Fig. 8). Statistical time series of the mean monthly precipitation analyzed for the wet season (June, July, August, and September) indicates that there was increased precipitation of about 60mm per month more in 2018. However, this made the soil moisture storage and retention potentially good for grass/vegetation or plant growth almost in the whole year except in the subsequent year

of 2019. Precipitation is one major limiting factor in MMNR particularly over and during the dry grazing period and whenever there is wildebeest migration from time to time. The rainfall pattern governs the biomass production and determines the growth of vegetation cover in the area. The spatial pattern of mean annual seasonal precipitation increases in the western or southwestern part of region similar to vegetation growth other than the spatial and temporal variability of rainfall. The wet season rainfall in MMNR is generally considered variable in quantity and distribution across the rangeland. However, several part of the regions receive good amount of rainfall while, the rest of the downstream receives low amount of rainfall.

3.2.4 Time series analyses of maximum mean monthly temperature for 2017-2019 period

During the period of 2017 to 2019, beside rainfall and vegetation variation, the analysis of mean monthly maximum temperature indicated that there was an increase in maximum temperature greater than $26^{o}C$ in almost completely dry season. In the months of January to March, however there was also a decrease from April to July, followed by gradual increase of temperature in the wet season particularly in July through October (Fig. 9). The immediate decrease of maximum temperature particularly in March or May end of dry season indicated the start of the main rainy season in almost the whole year. Although the variability of maximum temperature noticeable in both seasons, it is more visible in the extremely dry spell period than the normal season.

3.2.5 Time series analyses of mean monthly ndvi for the 2017- 2019 period

As observed from rainfall events, the erratic rainy season in dry season supported the soil store moisture that was utilized by vegetation such as shrubs, trees and grass growth in MMNR rangeland and the mean monthly NDVI time series results indicates an increase of NDVI value after dry season (Fig. 7). The spatial and temporal result of NDVI in the regime depicted an increase of vegetation grass cover in Mara Main particularly in August, whereas there was a minimum vegetation cover in Mara Bridge in the month of November, December, January, and February in almost the whole three years.
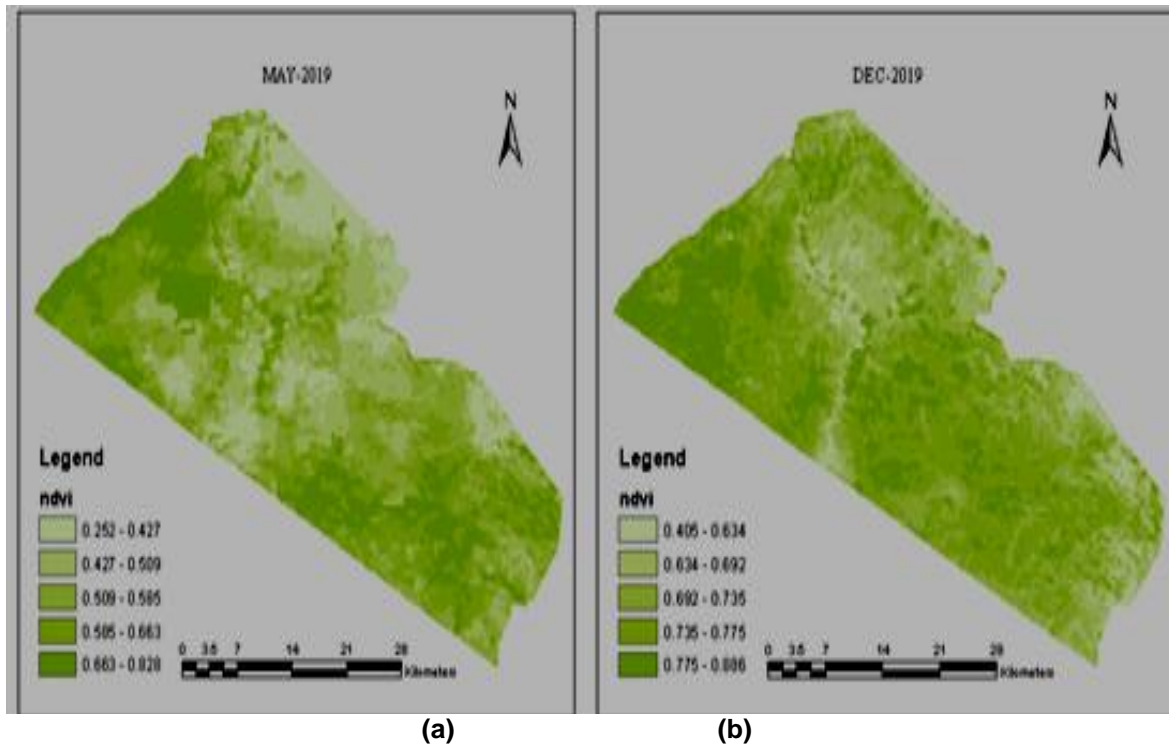
Fig. 7. Vegetation NDVI trend from MODIS imagery satellite data for Maasai Mara Rangeland wet (a) and dry (b) season acquired on (May and Dec 2019)

Fig. 8. Annual temperature and precipitation during the seasons

3.2.6 Statistical analysis of total aboveground standing biomass quantities

The sites grass biomass in MMNR indicates that maximum NDVI reflects the presence of maximum green biomass, while minimum reflects minimum green biomass. The different between maximum and minimum NDVI shows that biomass production varies depending on whether the season is dry or wet. As observed from most quadrat sites collection, generally, there was high vegetation cover in the wet season (March, April, May and July) than dry (January, February, short rains of August, September, October, November and December) from the period 2017 to 2019 as a result of good amount of rainfall in wet season for vegetation and grass growth. From the seasonal quantitative biomass of dry matter production harvested in dry and wet season, it can be noted that there is a significant differences that exist in production between bi-seasons clipped aboveground biomass as statistically shown in Tables 3 and 4.

17

3.3 Land Use Land Cover Change in Maasai Mara National Reserve Rangeland Ecosystems

In this study, maps were visualized based on each spatial coverage class of land use and land cover via MODIS derived images between 2009 and 2019. Generally, the major land use/covers in MMNR includes grassland, shrub-lands, rain-fed cropland, irrigated cropland, urban built-up bare land, water bodies, shrub-lands/natural grassland, forest cover (CEB), forest cover (CDB), forest cover (C - unknown), forest cover (OEB), forest cover (ODB) and forest cover (O-unknown) in the lower part of Maasai Mara catchment. Grasslands and shrub lands are mainly used for grazing of wildlife or as game reserves and encroachment of Maasai livestock herds. From these derived maps, it clearly appears that MMNR is predominantly occupied by large percentage of grassland with 46.8% (717km^2) in 2009, about 23.8% (365.4km^2), 15.8% (273km^2) of land being under closed forest with deciduous broadleaved respectively and natural grassland, as savannah, grasslands, or shrub lands, mostly used for grazing livestock and/or wildlife reserves. However, between 2009 and 2019, these rangelands have reduced by 3.379% (51.84km^2) due to encroached transformation of rain-fed cropland to irrigated cropland, whose area has increased from 0.82% (12.58km^2) to 4.20% (64.44km^2). Similarly, except for the grassland, shrub-land, forest cover, and water body, all the other land use/covers have undergone gradual change within the last decade under study. Similar observations were made by [40], they found that there are two systematic transitions (i.e., from closed forest to open forest and from open forest to small-scale agriculture) also reveal a trend (pathway) of deforestation from closed forest to small-scale agriculture, with open forest as a transitional land cover. This trend implies that closed forests are first opened up (probably for timber and charcoal) and then the opened patches are cultivated. Eventually, remaining trees are removed (logged) as cultivation expands into the open forest. The authors further observed that MMNR rangeland was intensively losing to mechanized agriculture between 1985 and 2003 attributed to a change of land tenure (from communal to private) especially in the rangeland.

Fig. 10 shows the LULC maps and respective proportion of cover occupied by each class between the year 2009 and 2011 of MMNR and rangeland ecosystem. The figure indicates that grassland occupies the largest proportion of the entire rangeland with 46.75%, which has remained constantly unchanged during the three-year period. Shrub-land with 23.82% has also remained unaltered in the same period and similarly the rest of the classes such as opened unknown forest cover (15.843%), rain-fed cropland (12.318%), forest cover closed unknown (0.819%) and irrigated cropland (0.064%) have been maintained in the entire ecosystem. The rain-fed and irrigated croplands are practiced in conservancies and some sections of Mara triangle where riparian Maasai community has encroached into the ecosystem for livelihood. This observation corroborated with a study conducted by [40], their results showed that livestock grazing as the predominant land use that changes with precipitation and land tenure leading to varying livelihood strategies. For example, agriculture is the most common livelihood in wet years and conservation levels increase with increasing support of wildlife conservation initiatives.

Fig. 9 shows a constant land use land cover class for grassland, shrubland, rainfed cropland and open unknown forest cover which had existed for the past three years since 2009 to 2012, however a decrease in land cover occurred between 2013 to 2015 for rainfed cropland from 12.32%, 11.79% to 10.33% and an increase of irrigated cropland from 0.588% in 2012 to 2.056% in 2015. This indicates the transformation of rainfed to irrigated cropland which signifies that some upcoming irrigation systems were being created in the area prompted by scarcity of rainfall. The authors [41] used MODIS time series data from 2000 to 2008 to develop expected annual greenness profiles for rangelands in southern Idaho to detect significant departures due to management changes or disturbance. Between 2003 and 2014, expansion of mechanized agriculture avoided gaining from rangelands systematically from small-scale agriculture. This implied that small plots are being used for smallholder agriculture in the rangeland are coalescing to larger plots for mechanized cultivation. The natural vegetation has been declining due to opening of natural rangelands to agricultural practices that expanded from rain-fed to irrigated croplands including inadequate conservation policies and implementation. LULC maps (Figures 9 to12) displays the base layer products for MMNR ecosystem.
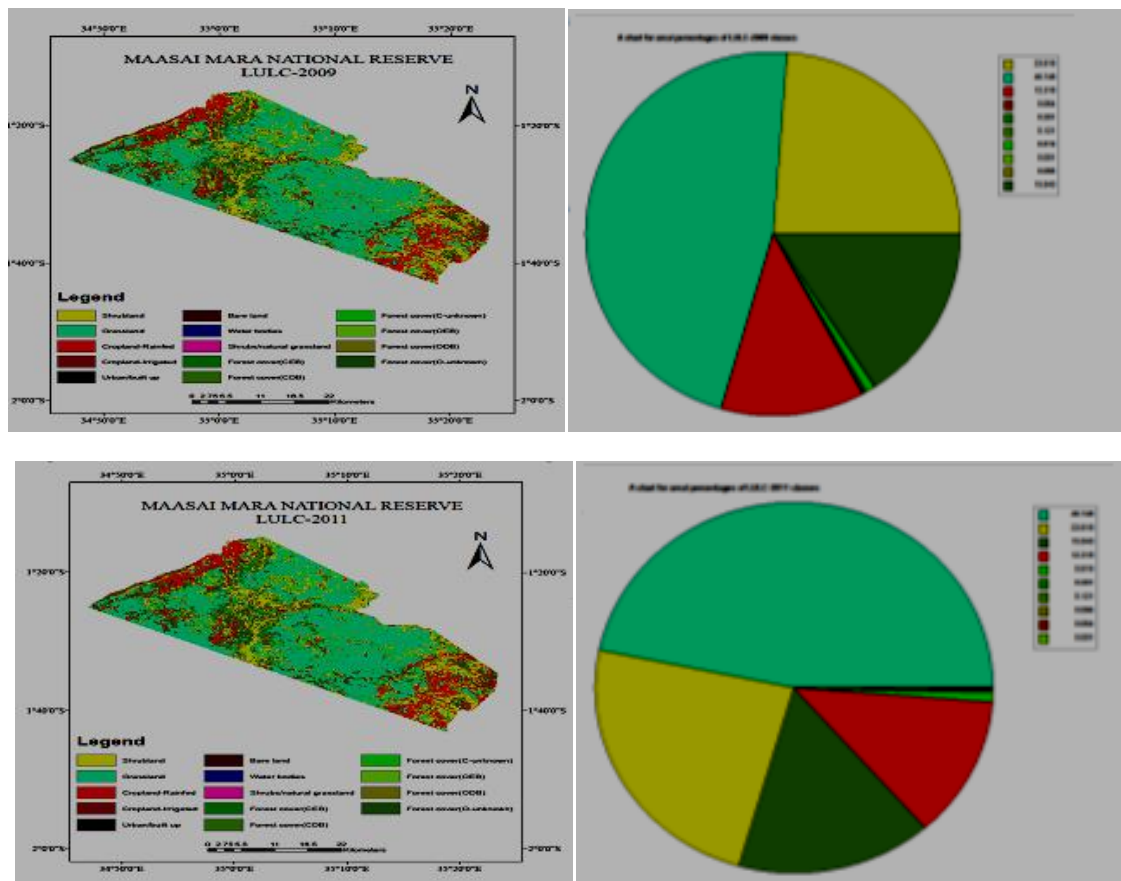
Fig. 9. Land use/cover classification maps using MODIS imagery data of Maasai Mara National Reserve from January 2009 through December 2011

Table 5. Maasai Mara National Reserve Land Use Land Cover classification between 2017- 2019 according to FAO land cover classes

OID	Class Name	Class Code	Count	Area cover (%)	Area cover (km^2)
0	**Shrubland**	**20**	**30162**	**23.818436**	**365.4163**
1	**Grassland**	**30**	**59199**	**46.748478**	**717.2031**
2	Cropland, rain-fed	41	10364	12.31824	188.9833
3	Cropland, irrigated	42	5316	0.063964	0.981319
4	Urban/built up area	112	254	0.20058	3.077247
5	Bare/sparse vegetation	114	153	0.120822	1.85362
6	Water bodies	116	1037	0.818902	12.56338
7	Shrubs/herbaceous cover	122	1	0.00079	0.01212
8	Forest (closed, evergreen broadleaved)	124	84	0.066333	1.017664
9	Forest (closed, deciduous broadleaved)	126	20063	15.84342	243.0657

The total area of MMNR is 1534.174313km^2

Fig. 11 shows the land use land cover classes of MMNR rangeland and ecosystem for three year period between 2017 and 2018, the maps and charts indicates that grassland has continued to remain untransformed with 46.75% similar to shrubland with 23.82%. This also applies to other land cover classes and open unknown forest cover, closed unknown forest cover with rainfed and irrigated croplands occupying the same area for the last decade.
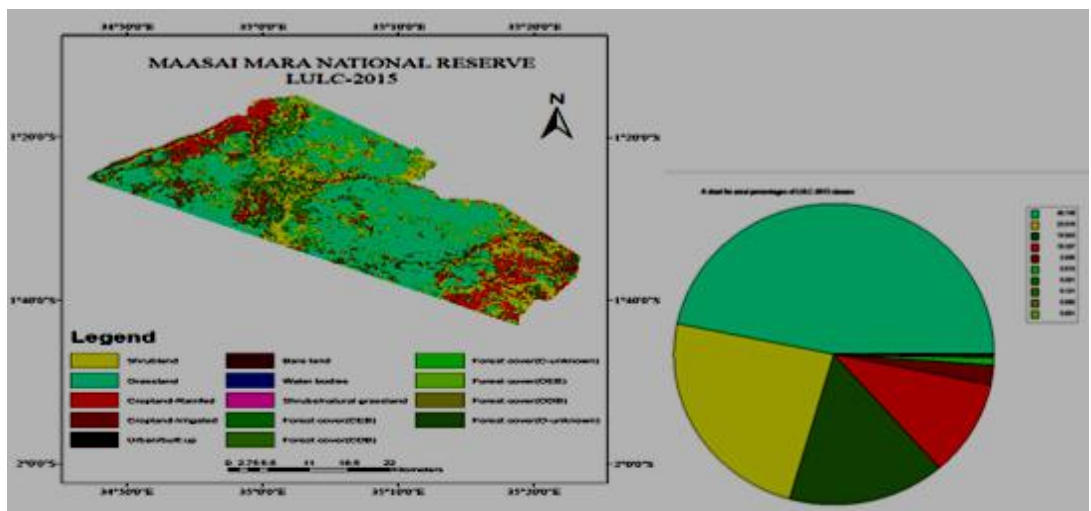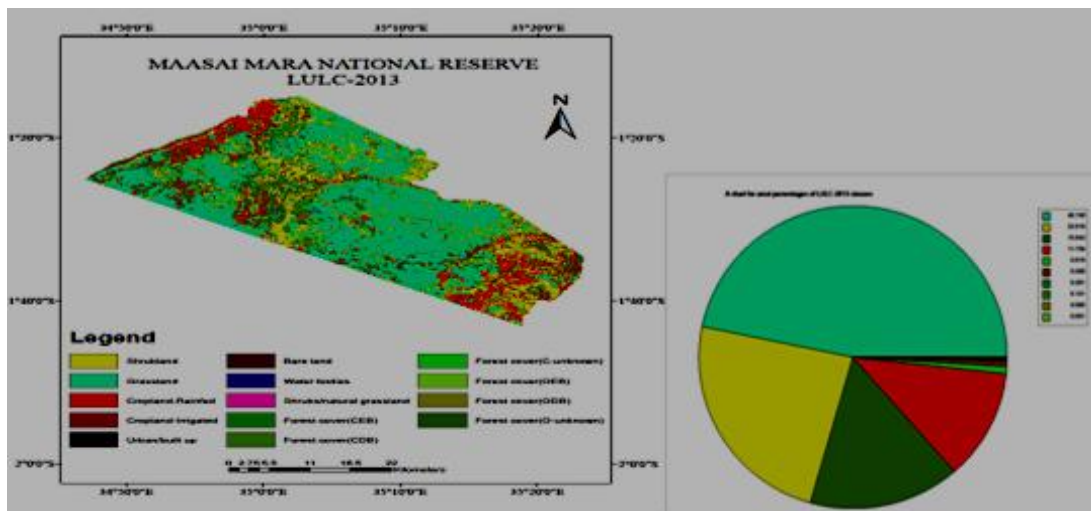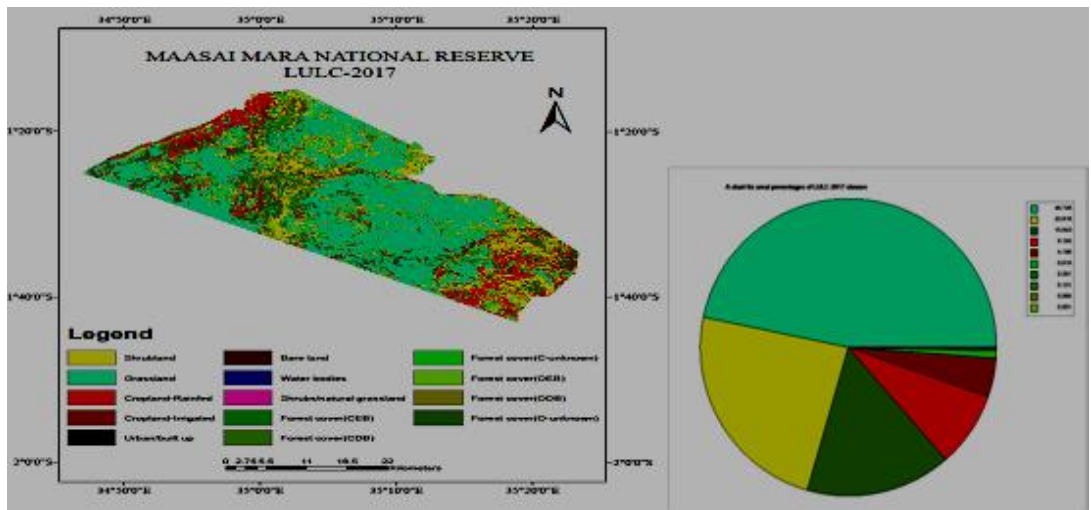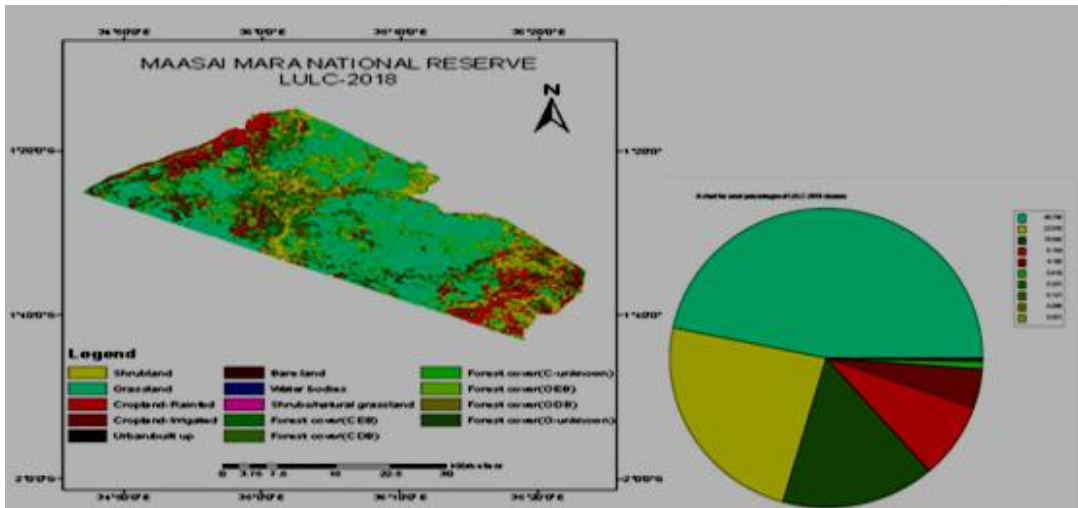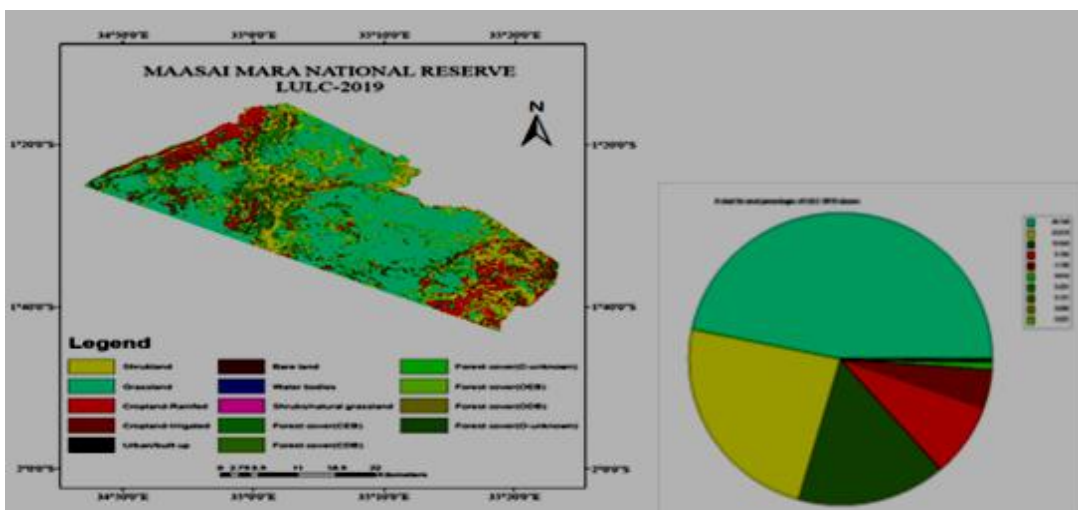
Fig. 10. Land use/cover classification maps of Maasai Mara National Reserve from 2013 through 2015 using MODIS imagery data

Fig. 11. Land use/cover classification maps of Maasai Mara National Reserve in 2017 through 2018 from MODIS imagery data

Fig. 12. Land use Land cover classification representation in percent for Maasai Mara rangeland ecosystem in 2019

Fig. 12 shows the LULC classes for the period 2019 and it can be observed that the grassland occupies the largest proportion of land cover followed with shrubs that takes 46.75% and 23.82% respectively. Land use Land cover has remained unchanged of some classes for the last decade except in the rain-fed cropland, which decreased in 2013 to 2015 from 12.32% to 10.33% because of transformed water managed or irrigated cropland. Due to short rains that were received in 2014, moving to irrigated cropland was probably the potential farming practices that were done in conservancies surrounding the MMNR ecosystem for food production. Most of the small-scale farmers alternatively shifted into

cultivation relying on rainfall and opted into venturing irrigation farming using water from excavated pans for storage of rainwater. The forest cover decreased from about 20% to about 7% of the study area between 1976 and 2014, which can be attributed to deforestation particularly in the Mau Forest the source of Mara River. The most notable change is the steady increase in small-scale agriculture and a decline in forest cover. During the same period, small-scale agriculture increased from approximately 6.5% to 21% of the landscape.

Table 5 shows the LULC classes for MMNR in area cover and its apparent that grassland dominates and occupies the greatest area of

717.203 km^2 (46.75%) of the total 1534.17km^2 followed by shrub-lands which are sparsely distributed within the entire rangeland catchment. Shrub-land occupies 365.4165km^2 (23.82%) with shrubs of herbaceous original with least area cover of 0.01212 km^2 (0.0008%). Closed deciduous broadleaved forest covers a substantive amount of cover, which was 243.07 (15.84%).

Table 6 shows direct expansion area estimation and it can be observed that coefficient of variation in the relationship between the ground truth and satellite images ranged between 3.004 and 6.483 and its relative efficiency was 4.657. Transformation of rain-fed cropping in cropland occupies 188.983km^2 (12.32%) which may have declined due to increased irrigated cropland with 0.981km^2 (0.064%) and built-up area occupying 3.08km^2 (0.2%) in the entire area.

3.3.1 Estimation of land cover and land use change

The estimation of land cover and land use was done at level I and level II where categories that were spatially and temporally similar were grouped under one class. The diversity of land use in the catchment was related to the diversity of agro climatic zones, landform, water resources, topography, and human activities. The dominant land use categories concentrated specifically on the agricultural application, which was considered the most important human economic activity in the area. Table 5 shows the major land cover classes identified based on [42].

3.3.2 Area estimation through direct expansion

This section presents the land cover generated maps resulting from the classification of satellite images, accuracy assessment of maps, magnitude determination including rates, nature and geographic distribution of land cover changes. The derived thematic maps of land cover types in MMNR were extracted from MODIS and Proba-V satellite images for the period of 2017, 2018, and 2019. Remote sensing techniques can be applied to perform crop area estimation by integrating area frame sampling

and classification of satellite images. The technique has been applied successfully by the national statistics service of US, department of agriculture during the 1980-1987 periods with satisfactory results [16]. The classification of rangeland ecosystem was divided into two major sub-classes, which appeared different as grassland and shrub-land because of their dissimilar spectral nature during classification process. The results obtained by direct expansion and regression estimation are shown in (Table 6).

3.3.3 Land classification accuracy assessment

In the study, accuracy assessment of ground truth was carried out for all land cover types using field surveys to ascertain how accurate the generated maps were in order to use the data more effectively and correctly. Satellite images from open access Copernicus hub was used to develop reference data products for comparison to land cover datasets, however field verification was performed by earlier conducting site visits enabling actual land cover comparison with land cover classifications dataset. Field verification data was compared to the classified land cover data, where the producer's accuracy, user's accuracy, and the overall accuracy were assessed in order to relate to each land cover categories. Accuracy was checked using the Kappa index of agreement, which is a measure for quantifying the level of agreement between two maps with equal number of classes. These accuracy measures are described in an error matrix (Table 7), where the land cover assessed in the field corresponds to the dataset classifications. The error matrices developed to assess the accuracies of the classifications indicated values between 80-100% for the producer's accuracy while user's accuracy ranged between 87.50-100% for MMNR. 3 out of 7 MODIS imagery maps (2017, 2018, and 2019) were assessed for accuracy using reference in-situ biomass data collected during fieldwork conducted in 2017, 2018 and 2019 in the ecosystem. The authors [43] secondly used 9 years of MODIS NDVI data to construct estimates of expected production for a southern Idaho study area and detect departures from this expectation.

Table 6. Maasai Mara National Reserve Land Cover and Land Use Statistics for 2017-2019

Land cover and Land use within segments	Total Surface Area (ha)		Variance	SE	CV	RE
Shrubland	Direct Expansion	6,173,224,354	561,202,214	7491.343	6.483	
	Regression Estimation	1,325,579,518	120,507,229	3471.415	3.004	4.657
Grassland	Direct Expansion	7,900,112,700	446,334,051	6680.824	2.946	
	Regression Estimation	8,238,406,919	481,778,182	6941.024	3.060	0.926
Cropland, rainfed	Direct Expansion	174,363,929	34,189,005.8	1849.027	3.094	
	Regression estimation	153,308,604	26,896,246	1640.008	2.744	1.271
Cropland, irrigated	Direct Expansion	700.354	962.987	9.81319	3.162	
	Regression estimation	310.299	620.592	7.877764	2.538	1.552
Urban/builtup Area	Direct Expansion	11,337.035	7,085.647	26.61888	2.735	
	Regression estimation	13,257.229	9,469.449	30.77247	3.162	0.748
Bare/sparse vegetation	Direct Expansion	10,994.903	3,435.9071	18.5362	3.162	
	Regression estimation	10,222.385	3,006.584	17.3395	2.958	1.143
Water bodies	Direct Expansion	631,354.068	157,838.517	125.6338	3.162	
	Regression estimation	596,111.817	141,931.39	119.135	2.999	1.112
Shrubs/herbaceous cover	Direct Expansion	0.170	0.284	125.6338	3.162	
	Regression estimation	0.0294	0.1469	0.1212	3.162	1.932
Forest(closed, evergreen broadleaved)	Direct Expansion	2,058.727	935.785	9.673598	3.060	
	Regression estimation	2,058.726	935.785	9.673598	3.006	1.000
Forest(closed, deciduous broadleaved)	Direct Expansion	57.299	6.6633	0.816258	0.979	
	Regression estimation	475.975	54.709	2.339012	3.043	0.122

V- Variance, SE – Standard Error, CV- Coefficient of Variation and RE – Relative Efficiency

Table 7. Maasai Mara National Reserve Rangeland Accuracy Assessment Report for Classification of MODIS image 2017, 2018, and 2019

Users	Class Producer's S	Gl	Cr	Ci	Bt	Bsv	Wb	Shc	F_{CEBI}	F_{CDBI}	Reference Totals
S	105	3	0	0	0	0	0	0	0	2	110
Gl	4	166	1	0	0	0	0	0	0	0	171
Cr	1	5	50	0	0	0	0	1	0	0	57
Ci	0	0	0	4	0	0	0	1	0	0	5
Bt	0	0	0	0	14	0	0	0	0	0	14
Bl	0	0	0	0	1	32	0	0	1	0	34
Wb	0	0	0	0	0	0	40	2	0	0	42
Sng	0	0	0	0	0	0	0	2	0	0	2
F_{CEBI}	0	0	0	0	1	0	0	0	21	0	22
F_{CDBI}	0	3	0	0	0	0	0	0	0	84	87
Classified Totals	110	177	51	4	16	32	40	6	22	86	518
Accuracy Assessment											
Producer's	95.45	93.79	98.04	100.00	87.50		100.00	100.00	100.00		95.45	97.67
User's	95.45	97.08	87.72	80.00	100.00		94.12	95.24	100.00		95.45	96.55
Kappa Class											
Overall Accuracy 95.22											
Kappa Index	0.94										

Confusion Matrix based on Test and Training Area (TTA) mask, S - Shrubland, G - Grassland, Cr – Cropland rain-fed, Ci – Cropland irrigated, Bt – Urban/built up, Bsv – Bare/sparse vegetation, Wb – Water bodies, Shc–Shrubland/herbaceous cover, F_{CEBI}- Forest Cover (Closed, evergreen broadleaved), F_{CDBI} – Forest cover (Closed Deciduous Broadleaved)

4. CONCLUSIONS

The sites grass biomass in MMNR indicates that maximum NDVI reflects the presence of maximum green biomass, while minimum reflects minimum green biomass. The different between maximum and minimum NDVI shows that biomass production varies depending on whether the season is dry or wet. As observed from most quadrat sites collection, generally, there was high vegetation cover in the wet season (March, April, May and July) than dry (January, February, short rains of August, September, October, November and December) from the period 2017 to 2019 as a result of good amount of rainfall in wet season for vegetation and grass growth. From the seasonal quantitative biomass of dry matter production harvested in dry and wet season, it can be noted that there is a significant differences that exist in production between bi-seasons clipped aboveground biomass. Rainfall behaviour influences the distribution of seasonal NDVI and the trend of carrying capacity of wildlife and livestock movement within the MMNR rangeland. Periods of fluctuating rainfall coupled with expansion of settlements, that is, mechanized cultivation for commercial wheat production like in the northern loita plains, encroachment of Maasai farmers and herders migrating from highly wheat potential areas of Naivasha cropland and Mau Narok in search of pasture, water, and charcoal burners etc. This may result in decline of biomass net primary productivity, which probably may cause drastic decline in wildlife population in the rangeland ecosystem with subsequent decline in tourism as a revenue generators for both National and county governments. In a study conducted by [44], they observed that wildlife populations will fall by at least 40% and that certain species of wildlife attractive to tourism such as rhinos, carnivores, and eland may disappear/extinct entirely from the Maasai Mara rangelands. The large-scale use of satellite-based NDVI products as an input for studies associated with biomass productivity and anomalies should consider the anisotropy effects of this vegetation index. The thematic maps results showed that MODIS and Proba-V images could be used to produce land use/cover maps and statistics for maximum likelihood classification (MLC). These values were used as the measure of actual agreement and the expected output in the sense that values within these ranges usually gives an indicator to good representations of the actual land use and land cover. The study recommends that in-situ quantification of AGGB may not be the actual biomass as with the corresponding NDVI values obtained through satellite images, future work requires research based on spatio-temporal quantification of biomass which may provide realistic assessment of biomass trend in wet and dry season and to validate real-time vegetation phenology in rangeland ecosystem.

DISCLAIMER

COMPETING INTERESTS

Authors have declared that no competing interests exist.

REFERENCES

1.   Smith P, Lanigan G, Kutsch WL, Buchmann N, Eugster W, Aubinet M, Jones M. Measurements necessary for assessing the net ecosystem carbon budget of croplands, Agricultural Ecosystem. & Environment. 2010;139: 302–315.
     DOI:10.1016/j.agee.2010.04.004.
2.   Asner GP, Elmore AJ, Olander LP, Martin RE, Harris AT. Grazing systems, ecosystem responses, and global change. Annual Review of Environment and Resources. 2004;29:261-299.
3.   Mbatha KR, Ward D. The effects of grazing, fire, nitrogen and water availability on nutritional quality of grass in semi-arid savanna, South Africa. Journal of Arid Environment. 2010;74(10):1294–1301.
     DOI: 10.1016/j.jaridenv.2010.06.004.
4.   Ontitism SM, Ondabu N, Ouda J. The performance and composition of ley grasses and legumes, sweet potatoes and fodder trees. In: Wamae L, Murithi F, Wasike W (eds) Proceedings of the 7th KARI biennial scientific conference held on 13th–17th November 2000, Nairobi. 2000;389–392.
5.   Reeves MC, Zhao M, Running SW. Applying improved estimates of MODIS

productivity to characterize grassland vegetation dynamics. Rangeland Ecology and Management. 2006;59:1–10.

6. Ozyavuz M, Bilgili BC, Salici A. Determination of vegetation changes with NDVI method. Journal of Environmental Protection and Ecology. 2015;16(1):264–273.

7. Biondini ME, Patton BD, Nyren PE. Grazing intensity and ecosystem processes in a northern mixed-grass prairie, USA. Ecological Applications. 1998;8:469-479.

8. Stohlgren TJ, Schell LD, VandenHeuvel B. How grazing and soil quality affect native and exotic plant diversity in rocky mountain grasslands. Ecological Applications. 1999;9:45-64.

9. Arevalo JR, de Nascimento L, Fernandez-Lugo S, Mata J, Bermejo L. Grazing effects on species composition in different vegetation types (La Palma, Canary Islands). ActaO ecologica International Journal of Ecology. 2011;37:230-238.

10. Waithaka J. Maasai Mara - an ecosystem under siege: an African case study on the societal dimension of rangeland conservation, African Journal of Range and Forage Science, 2004;21:2:79-88. DOI: 10.2989/10220110409485838.

11. Olson RJ, Johnson KR, Zheng DL, Scurlock JMO. Global and Regional Ecosystem Modeling: Databases of Model Drivers and Validation Measurements. ORNL Technical Memorandum TM-2001/196. Oak Ridge National Laboratory, Oak Ridge, Tennessee; 2000.

12. Comber AJ, Fisher PF, Wadsworth RA. What is land cover? Environment and Planning and Design. 2006;32(2): 199-209.

13. Madana M. Improving land use survey method using high-resolution satellite imagery. International Institute for Geo Information Science and Earth Observation (ITC) (M.Sc. Thesis); 2002.

14. Fonseca F, De Figueiredo T, Nogueira C, Queirós A. Effect of prescribed fire on soil properties and soil erosion in a Mediterranean mountain area. Geoderma. 2017;307:172–180.

15. Cochran WG. Sampling techniques (3rd ed.). New York: John Wiley & Sons; 1977.

16. Allen JD, Hanuschak GA. The Remote Sensing Applications Program of the National Agricultural Statistics Service 1980-1987. National Agricultural Statistics Service staff report no. SRB-88-08, United States Department of Agriculture, National Agricultural Statistics Service; 1988.

17. Francois M, Santandrea S, Mellab K, Vrancken D, Versluy J. The PROBA-V mission: The space segment. International journal of Remote Sensing. 2014;35:2548-2564. DOI: 10.1080/01431161.2014.883098.

18. Thuillier G, Hersé M, Foujols T, Peetermans W, Gillotay D, Simon PC, Mandel H. The solar spectral irradiance from 200 to 2400 nm as measured by the SOLSPEC spectrometer from the ATLAS and EURECA missions. Solid Physics. 2003;214:1–22. DOI: 10.1023/A: 1024048429145.

19. Rahman H, Dedieu G. SMAC: a simplified method for the atmospheric correction of satellite measurements in the solar spectrum. Remote Sensing. 1994;15(1): 123-143.

20. Plummer S, Chen J, Dedieu G, Simon M. GLOBCARBON Detailed Processing Model GLBC-ESL-DPM-V1.3. 2003;202.

21. Berthelot B, Dedieu G, Cabot F, Adam S. "Estimation of surface reflectance's and vegetation index using NOAA/AVHRR: Methods and results at global scale", Communications for the 6th International Symposium on Physical Measurements and Signatures in Remote Sensing, Val d'Isère, France, January. 1997:17-21.

22. Brandt M, Romankiewicz C, Spiekermann R, Samimi C. Environmental change in time series-an interdisciplinary study in the Sahel of Mali and Senegal. Journal of Arid Environments. 2014;105:52–63.

23. Committee on Environment and Natural Resources. Our Changing Planet: The FY 1995 U.S. Global Change Research Program. Washington, DC: National Science and Technology Council; 1995.

24. Running SW, Ramakrishna NR, Heinsch FA, Zahao M, Reeves M, Hashimoto H. A continuous satellite-derived measure of global terrestrial primary production. Bioscience. 2004;54:547-560.

25. Janetos AC, Justice CO. Land cover and global productivity: A measurement strategy for the NASA programme, International Journal of Remote Sensing. 2000;21:6-7:1491-1512. DOI: 10.1080/014311600210281.

26. Skole DL, Justice CO, Townshend JRG, Janetos AC. 'A land cover change monitoring program: Strategy for an international effort', Mitigation Adaptation. Strategic Global Change. 1997;2:157–175.

27. Drusch M, Del Bello U, Carlier S. Sentinel-2: ESA's optical high-resolution mission for GMES operational services. Remote Sensing Environment. 2012;120:25-36.

28. Franch B, Vermote EF, Becker-Reshef I. Improving the timeliness of winter wheat production forecast in the United States of America, Ukraine and China using MODIS data and NCAR Growing Degree Day information. Remote Sensing of Environment. 2015;161:131-148.

29. Latham JS. Final report of a pilot project on the utilization of Remote Sensing and Field data for the production of Agricultural statistics on crop acreage. Unpublished internal report, FAO; 1981-83.

30. Wigton W, Srivastava A, Zekaria S, Mudeir Y, Mossa Y, Tadesse G, Abdi J. Agricultural Statistical Methodology in Ethiopia. Central Statistical Agency (Ethiopia) Publication: Addis Ababa; 2009.

31. Nemani PR, Running SW. Estimation of regional surface resistance to evapotranspiration from NDVI and thermal IR AVHRR data. Journal of Applied Meteorology. 1989;28:276- 284.

32. Zhou LM, Tucker CJ, Kaufmann RK, Slayback D, Shabanov NV, Myneni RB. Variations in northern vegetation activity inferred from satellite data of vegetation index during 1981 to 1999. Journal of Geophysical Research and Atmosphere. 2001;106:20069–20083.

33. Buitenwerf R, Rose L, Higgins SI. Three decades of multi-dimensional change in global leaf phenology. National Climate Change. 2015;5:364–368.

34. Baldyga TJ. Assessing land cover change impacts in Kenya's River Njoro watershed using remote sensing and hydrologic modeling (Master's thesis). Laramie: University of Wyoming; 2005.

35. Congalton RG. A review of assessing the accuracy of classifications of remotely sensed data. Remote Sensing of Environment. 1991;37:35-46.

36. Foody GM. Status of land covers classification accuracy assessment. Remote Sensing of Environment. 2002;80: 185–201.

37. Stehman SV. "Selecting and interpreting measures of thematic classification accuracy." Remote Sensing of Environment. 1997;62:77-89.

38. Mwangi H, Lariu M, Padia Julich, Stefan Patil, Sopan D, Mcdonald, Karl-einz. Characterizing the Intensity and Dynamics of Land-Use Change in the Mara River Basin, East Africa. 2017;9:8.
DOI: 10.3390/f9010008.

39. Browning DM, Franklin J, Archer SR, Gillan JK, Guertin DP. Spatial patterns of grassland-shrubland state transitions: A 74 year record on grazed and protected areas. Ecological Applications. 2014;24: 1421–1433.

40. Kariuki, Rebecca Willcock, Simon Marchant, Rob. Rangeland livelihood strategies under varying climate regimes: Model insights from southern Kenya. Journal of Land Management. 2018;7(47): 1-22.
DOI: 10.3390/land7020047.

41. Wylie BK, Boyte SP, Major DJ. Ecosystem performance monitoring of rangelands by integrating modeling and remote sensing. Rangeland Ecology and Management. 2012;65:241–252.

42. Anderson JR. Land use and land cover changes: A framework for monitoring. Journal of Research by the Geological Survey. 1977;5:143-153.

43. David D, Briske Walker, Lawrence R. Rangeland systems processes, management and challenges. Rangeland systems in developing nations: conceptual advances and societal implications Rangeland Systems ed D D Briske (Cham: Springer Series on Environmental Management). 2017;1(12): 569–642.
DOI:10.1007/978-3-319-46709-2.

44. Reid RS, Rainy M, Ogutu J, Kruska RL, Kimani K, Nyabenge M, Lamprey R. People, Wildlife and Livestock in the Mara Ecosystem: the Mara Count 2002. Report, Mara Count 2002. International Livestock Research Institute, Nairobi, Kenya; 2003.